Acta Crystallographica Section D
Biological Crystallography
ISSN 0907-4449

How RhoGDI binds Rho

Kenton Longenecker,[a]† Paul Read,[a]† Urszula Derewenda,[a] Zbigniew Dauter,[b] Xiaopu Liu,[a] Sarah Garrard,[a] Lori Walker,[a] Avril V. Somlyo,[a] Robert K. Nakamoto,[a] Andrew P. Somlyo[a] and Zygmunt S. Derewenda[a]*

[a]Department of Molecular Physiology and Biological Physics, University of Virginia Health Sciences Center, Charlottesville, VA 22906, USA, and [b]National Cancer Institute, Frederick and Brookhaven National Laboratory Building 725A-X9, Upton, NY 11973, USA

† These authors contributed equally to the project.

Correspondence e-mail: zsd4n@virginia.edu

Received 29 April 1999
Accepted 15 June 1999

PDB Reference: RhoA–RhoGDI complex, 1cc0.

Like all Rho (Ras homology) GTPases, RhoA functions as a molecular switch in cell signaling, alternating between GTP- and GDP-bound states, with its biologically inactive GDP-bound form maintained as a cytosolic complex with RhoGDI (guanine nucleotide-exchange inhibitor). The crystal structures of RhoA–GDP and of the C-terminal immunoglobulin-like domain of RhoGDI (residues 67–203) are known, but the mechanism by which the two proteins interact is not known. The functional human RhoA–RhoGDI complex has been expressed in yeast and crystallized ($P6_522$, unit-cell parameters $a = b = 139$, $c = 253$ Å, two complexes in the asymmetric unit). Although diffraction from these crystals extends to 3.5 Å and is highly anisotropic, the experimentally phased (MAD plus MIR) electron-density map was adequate to reveal the mutual disposition of the two molecules. The result was validated by molecular-replacement calculations when data were corrected for anisotropy. Furthermore, the N-terminus of RhoGDI (the region involved in inhibition of nucleotide exchange) can be identified in the electron-density map: it is bound to the switch I and switch II regions of RhoA, occluding an epitope which binds Dbl-like nucleotide-exchange factors. The entrance of the hydrophobic pocket of RhoGDI is 25 Å from the last residue in the RhoA model, with its C-terminus oriented to accommodate the geranylgeranyl group without conformational change in RhoA.

1. Introduction

RhoA, a member of the Ras-homology family of regulatory cytosolic GTPases, plays major roles in multiple cellular processes, including organization of the cytoskeleton (Mackay & Hall, 1998; Narumiya *et al.*, 1997), cytokinesis (Narumiya, 1996), organogenesis (Wissmann *et al.*, 1997), tumor invasiveness (Itoh *et al.*, 1999; Yoshioka *et al.*, 1998), neurite retraction and growth-cone organization (Jalink *et al.*, 1994; Luo *et al.*, 1997), exocytosis (Mariot *et al.*, 1996; Norman *et al.*, 1996), smooth muscle contraction and, through this mechanism, hypertension (Gong *et al.*, 1996; Uehata *et al.*, 1997). RhoA assumes the biologically active conformation upon binding of GTP and reverts to an inactive state when GTP is hydrolyzed to GDP. This cycle is regulated by accessory proteins, such as GAPs (GTPase-activating proteins), which dramatically enhance the rate of GTP hydrolysis (Gamblin & Smerdon, 1998; Scheffzek, Ahmadian & Wittinghofer, 1998), and GEFs (guanine nucleotide-exchange factors), which catalyze the exchange of GDP with GTP (Pan & Wessling-Resnick, 1998). Nucleotide exchange and *in vivo*

activation of effectors of RhoA are accompanied by (and probably require) its association with the plasma membrane through the prenylated RhoA C-terminus (Bokoch *et al.*, 1994; Fujihara *et al.*, 1997; Gong *et al.*, 1996; Gong, Fujihara, Somlyo *et al.*, 1997; Gong, Fujihara, Walker *et al.*, 1997; Nomanbhoy & Cerione, 1996). Most of RhoA present in resting cells is complexed with the guanine nucleotide-exchange inhibitor RhoGDI (Fukumoto *et al.*, 1990; Bourmeyster *et al.*, 1992). Translocation to the membrane and possibly nucleotide exchange are dependent on the dissociation of RhoA from RhoGDI. Of the three isoforms of RhoGDI identified to date, RhoGDIa, henceforth referred to simply as RhoGDI, is expressed ubiquitously and interacts with all three key Rho GTPases, including RhoA, Cdc42Hs and Rac (Adra *et al.*, 1998; Sasaki & Takai, 1998).

Structural studies have only recently begun to unravel some of the complex details of Rho-mediated cell regulation (Sprang, 1997). RhoA has been studied by X-ray crystallography in complex with GDP (Wei *et al.*, 1997) and with bound GTPγS (Ihara *et al.*, 1998). Cdc42Hs has been characterized by NMR (Feltham *et al.*, 1997) in both the active and inactive conformations. A structure of Rac in the active conformation was determined by X-ray crystallography (Hirshberg *et al.*, 1997). The details of the mechanism by which Rho-specific GAPs enhance the rate of GTP hydrolysis were inferred from crystallographic studies (Barrett *et al.*, 1997; Nassar *et al.*, 1998; Rittinger, Walker, Eccleston, Nurmahomed *et al.*, 1997; Rittinger, Walker, Eccleston, Smerdon *et al.*, 1997; Scheffzek, Ahmadian, Weismuller *et al.*, 1998).

The mechanistic aspects of the interactions of Rho GTPases with their GEFs and RhoGDI are not well understood. Rho-specific GEFs typically contain a Dbl-like domain in tandem with a PH domain. The structure of such a two-domain fragment from the human SOS protein has been reported (Soisson *et al.*, 1998), but its mechanism is unclear. RhoGDI has been studied in its native form only, both by crystallography and NMR (Gosser *et al.*, 1997; Keep *et al.*, 1997). It is a 204-residue protein which is only partly folded in the absence of the GTPase. The globular domain, amino acids 69–203, has a structure reminiscent of the immunoglobulin fold (Gosser *et al.*, 1997; Keep *et al.*, 1997). The ΔN59 variant of the protein binds well to the GTPase with an almost unaffected affinity, but does not inhibit nucleotide-exchange properties. Consequently, the inhibitory function resides in the N-terminus.

In this paper, we report an X-ray diffraction study of crystals of the human RhoA–RhoGDI complex obtained by co-expression of the two full-length proteins in *Saccharomyces cerevisiae*. These crystals diffract X-rays poorly, with significant anisotropy, and do not allow for the refinement of an atomic model. Nonetheless, the experimentally phased (MAD plus MIR) electron-density map at 5 Å clearly reveals the mutual disposition of RhoA–GDP and RhoGDI in the complex and suggests a mechanism by which the N-terminal fragment of RhoGDI fulfills its biological role.

2. Experimental

2.1. Preparation of recombinant samples for crystallization

To enhance the chances of obtaining well diffracting crystals, we prepared samples of complexes of N-terminally tagged and untagged proteins. Tagged human RhoA and RhoGDI, both full length, were co-expressed in yeast strain SY1 (Nakamoto *et al.*, 1991) transformed with multicopy 2μ plasmids carrying the cDNA under control of the inducible GAL1 promoter. The open reading frames were modified with either a His_6 or FLAG affinity tag at the amino termini. Approximately half of the FLAG-tagged RhoA protein was found to be membrane associated, indicating that it was properly modified by addition of geranylgeranyl at the cysteine in the carboxyl-terminal sequence CLVL. The other half of the FLAG-tagged RhoA was found in the cytosolic fraction, most of which was in complex with $(His)_6$-tagged RhoGDI. The FLAG–RhoA/$(His)_6$–RhoGDI complex which was used to grow crystals was purified directly from the cytosolic fraction by sequential passage over a Talon metal-affinity column (Clonetech) followed by an anti-FLAG M2 monoclonal antibody column (Kodak). The heterodimer was very stable, eluting as a single peak from an anion-exchange column as well as from a Superdex 75 (Pharmacia) gel-filtration column. Yields of 4–5 mg from 18 l of culture were regularly obtained. The final protein sample was concentrated to 10–15 mg ml^{-1} using an Amicon 10 centrifuge concentrator.

The untagged samples were obtained using N-terminally tagged (His_6)RhoA expressed in sf9 cells using the pFastBac system (Life Technologies), solubilized by the addition of 90% pure *E. coli* expressed RhoGDI, either in its full-length form or with the N-terminal 22 residues truncated (Sheffield *et al.*, 1999). However, this approach did not yield crystals.

2.2. Enzymatic assays

Protein-associated nucleotides were quantitated by separation over a Waters HPLC SAX column, and elution followed at 254 nm with integration of the peaks compared with standards (Gong *et al.*, 1996). Protein concentrations were determined using the Bio-Rad protein assay. The stability of bound GDP in the FLAG–RhoA/(His_6)–RhoGDI complex was determined by incubation of 0.1 m*M* purified complex in 0.1 *M* Tris–HCl, 0.1 *M* NaCl and 5 m*M* $MgCl_2$ pH 8.0 at 295 K. At selected times, 20 µl samples were diluted 20-fold and then concentrated to remove any released nucleotide. The protein concentration of the samples were determined, the protein was precipitated with 1% perchloric acid and the concentration of GDP remaining in the supernatant was determined by HPLC.

2.3. Crystallization and preparation of derivatives

Crystals were obtained regardless of the order of the affinity tags. Data reported here are for the FLAG–RhoA–His_6–RhoGDI crystals. The largest crystals were grown by vapor diffusion in sitting drops using equal volumes of protein (15 mg ml^{-1} in 25 m*M* Tris–HCl pH 8.0, 100 m*M* NaCl, 5 m*M*

Table 1
X-ray data collection.

Values in parentheses are for the highest resolution shell.

Data	Native	Hg	Ho^{3+} (edge)	Ho^{3+}(peak)	Ho^{3+} (remote)
Source	EMBL-BW7B	APS-19ID	NSLS-X9B	NSLS-X9B	NSLS-X9B
Wavelength (Å)	0.8373	1.0084	1.5342	1.5333	1.5212
d_{min} (Å)	4.0	4.5	5.0	5.0	5.0
Total observations	130318	63220	27760	28099	27478
Unique observations	12817	9016	6644	6648	6655
Completeness (%)	99.1 (99.6)	98.5 (99.2)	99.2 (94.5)	99.4 (95.6)	99.5 (98.1)
$I/\sigma(I)$	12.1	8.8	14.9	12.5	14.0
R_{sym}† (%)	6.1 (19.3)	9.0 (19.3)	8.5 (16.7)	11.0 (24.2)	8.6 (23.5)
R_{iso}‡ (%)	—	25.2	20.2	—	—

† $R_{sym} = \sum|I - \langle I\rangle|/\sum I$, where I is the integrated intensity for a particular reflection. ‡ $R_{iso} = \sum|F_{PH} - F_P|/\sum F_P$, where F_{PH} and F_P are the scaled structure-factor amplitudes of the derivative and native.

$MgCl_2$) and reservoir solution [51% saturated $(NH_4)_2SO_4$, 100 m*M* CH_3COONa pH 5.3] and overlaying the drops with oil (50% paraffin/50% silicon). Transfer to the final stabilization solution [53% saturated $(NH_4)_2SO_4$, 100 m*M* CH_3COONa pH 5.3, 5 m*M* $MgCl_2$ and 27%(*w*/*v*) xylitol] for flash-freezing was achieved gradually, with 5% increments of xylitol over a period of 30–45 min. Crystals were frozen in liquid nitrogen and stored or frozen directly in a cold stream at the beamline. They exhibited the symmetry of space group $P6_522$ (or $P6_122$), with unit-cell parameters $a = b = 139$, $c = 253$ Å. The Hg derivative was produced by soaking a crystal in 1 m*M* thiomersal, 53% saturated $(NH_4)_2SO_4$, 100 m*M* CH_3COONa pH 5.3, 5 m*M* $MgCl_2$ for 5 h. The Eu and Ho derivatives were prepared by soaking crystals in either 2 m*M* $EuCl_3$ or 2 m*M* $HoCl_3$, 53% saturated $(NH_4)_2SO_4$, 100 m*M* CH_3COONa pH 5.3 for 70 h.

2.4. Data collection

Data sets were collected on three different synchrotron beamlines (Table 1). The native data were collected on a MAR Research 345 detector using beamline BW7B at the EMBL Outstation, Hamburg, Germany. The Hg derivative set was collected with the 3×3 CCD detector on beamline 19-ID(SBC) at the Advanced Photon Source, Argonne National Laboratory. The three-wavelength MAD experiment was conducted on an ADSC 2×2 CCD detector using beamline X9B at the National Synchrotron Light Source, Brookhaven National Laboratory. Diffraction data were integrated and scaled using the *HKL* suite (Otwinowski & Minor, 1997). Unless specified otherwise, subsequent calculations utilized programs implemented in the *CCP*4 package (Collaborative Computational Project, Number 4, 1994) or the *X-PLOR* and *CNS* suites (Brunger *et al.*, 1998). Intensities were converted to structure-factor magnitudes using *TRUNCATE* (Collaborative Computational Project, Number 4, 1994), which also calculated the fall-off in the structure-factor magnitudes for orthogonal directions.

2.5. Experimental phase determination

The unit-cell volume of the crystals suggested either two or three complexes in the asymmetric unit, but non-crystallographic symmetry was not found. Initial molecular-replacement (MR) calculations using the atomic coordinates of RhoA–GDP (PDB code 1ftn, residues 4–180) and RhoGDI (PDB code 1rho, residues 68–203 of chain *A*) did not produce a convincing solution and it was therefore necessary to resort to experimental phasing. A putative Hg derivative was identified early on and data to 4.5 Å were used to search for the Hg positions. Unfortunately, neither direct-methods nor Patterson searches were successful in establishing the positions of the metal atoms. The phases were eventually determined by a combination of multiwavelength anomalous dispersion (MAD) and multiple isomorphous replacement (MIR) techniques. It was known to us from studies of RhoA (Wei *et al.*, 1997) that Eu^{3+} can replace Mg^{2+} in RhoA–GDP. A low-resolution experiment conducted in-house revealed that the same substitution can take place in the crystals of the complex, yielding an interpretable isomorphous-difference Patterson map revealing two sites (data not shown). This opened the avenue of a MAD experiment – the SeMet option was not feasible because of the yeast expression system – but the L_{III} absorption edge of Eu at 1.776 Å was not deemed practical, so we opted for Ho^{3+}, which has the L_{III} edge at higher energy (1.537 Å). A fluorescence scan of the Ho^{3+} derivative showed an intense white line and allowed the selection of three wavelengths for the MAD experiment. Since the crystals of the Rho–RhoGDI complex diffract poorly, we have restricted the experiment to 5 Å resolution. The heavy-atom structure in the Ho derivative was solved with *SHELXS* (Sheldrick & Gould, 1995) using either anomalous differences or dispersive differences (Table 2; Fig. 1). In spite of the poor quality of the data, the MAD phases, improved by solvent flattening, allowed us to calculate an electron-density map ($P6_522$ was identified at this point as the correct space group) in which the boundaries of two complexes and the orientation of the RhoA molecules could clearly be identified. This revealed twofold

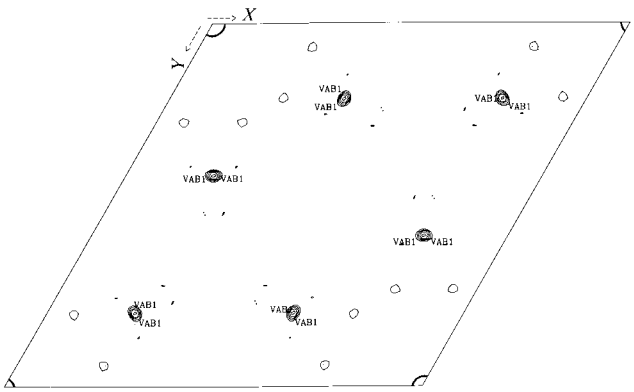

Figure 1
Anomalous difference Patterson for the Ho derivative. The $W = 0$ section is contoured at 1σ intervals, beginning at the 3σ level.

Table 2
Heavy-atom structures.

MAD data. Interatomic distance between sites *A* and *B* is 49.2 Å.

	x	y	*z*
Ho^{3+} site *A*	0.766	0.392	0.072
Ho^{3+} site *B*	0.175	0.578	0.075

	Occupancy† (real/anomalous)	
	Site *A*	Site *B*
Ho^{3+} (edge)	—/1.85	—/1.67
Ho^{3+} (peak)	0.23/3.23	0.20/2.85
Ho^{3+} (remote)	0.22/1.77	0.19/1.56

MIRAS data	*x*	*y*	*z*	Occupancy† (real/anomalous)
Ho^{3+} site *A*	0.761	0.386	0.072	0.80/1.55
Ho^{3+} site *B*	0.177	0.584	0.076	0.59/1.38
Hg site *A*	0.378	0.548	0.169	0.59/—
Hg site *B*	0.586	0.480	0.171	0.38/—
Hg site *C*	0.368	0.562	0.261	0.19/—
Hg site *D*	0.598	0.478	0.262	0.20/—

† Values refined using a constant temperature factor of $B = 20$ Å^2.

non-crystallographic symmetry (NCS) and indicated a solvent content of 66%. The local dyad nearly coincides with the crystallographic twofold screw axis, which explains why the self-rotation function failed to detect non-crystallographic symmetry. Subsequently, a native Patterson map revealed a translational peak expected from the nearly parallel orientations of the crystallographic and non-crystallographic symmetry axes.

The MAD phases were used to detect four metal sites in the Hg derivative (Table 2; Fig. 2). The metal substructure had a twofold symmetry consistent with the MAD-phased electron-density map. Another set of phases (MIRAS) was then calculated based on isomorphous and anomalous differences, using the Ho^{3+} (edge) and the Hg data sets. The choice of Ho^{3+} (edge) over Ho^{3+} (peak) was dictated by the higher $I/\sigma(I)$ ratio in the former data set, which was expected to yield better estimates of isomorphous differences. Combination of the MIRAS and MAD phases, using *SIGMAA* followed by *DM* (Collaborative Computational Project, Number 4, 1994), produced an electron-density map which was used in the *RAVE* program suite (Kleywegt & Jones, 1994) to calculate the correlation about the non-crystallographic dyad in the electron-density map and also in the calculation of molecular envelopes. The final experimentally phased 5 Å resolution map utilized phases calculated in *DM* with NCS averaging (Table 3; Fig. 3). This map confirmed the location of the RhoA model and allowed the positioning of the C-terminal domain of RhoGDI. The mutual disposition of the two proteins RhoA (residues 4–180) and RhoGDI (residues 68–203) was further refined by rigid-body refinement in real space, using the program *O* (Jones *et al.*, 1991).

The residual electron-density map, used to visualize the putative conformations of the N-terminus of RhoGDI and of the C-terminus of RhoA, was prepared by subtracting a map extracted from within a mask covering the coordinates of the nucleotide-free RhoA and RhoGDI molecules from a map extracted using the mask used for NCS averaging.

2.6. Molecular replacement

The positioning of the RhoA molecules in the crystal was facilitated by the easily interpretable configuration of the α-helices and was further validated by the chemistry of the Ho^{3+} and Hg^{2+} derivatives. However, no such validation was at hand for RhoGDI, which being a β-barrel is not easily interpretable at 5.0 Å resolution and which contained no heavy-atom binding sites. In an effort to independently validate the orientation of RhoGDI, using intensity data as opposed to experimental phases, we resorted to MR calculations using *AMoRe* (Navaza, 1994; Table 4). A rotational search with the full model was performed using all reflections between 10 and 5.0 Å, the range of data which yielded the highest signal for the top solution. All solutions output from the rotational search were fed into the translational search, which utilized data between 20 and 4.5 Å, and the top solution for each orientation was subjected to rigid-body refinement against data between 15 and 4.5 Å. A similar procedure was performed for the calculations with the individual components of the structure. To reconstruct the model of the complex from its individual protein components, calculations were performed both with uncorrected native data and data adjusted to account for the anisotropy. The overall anisotropic

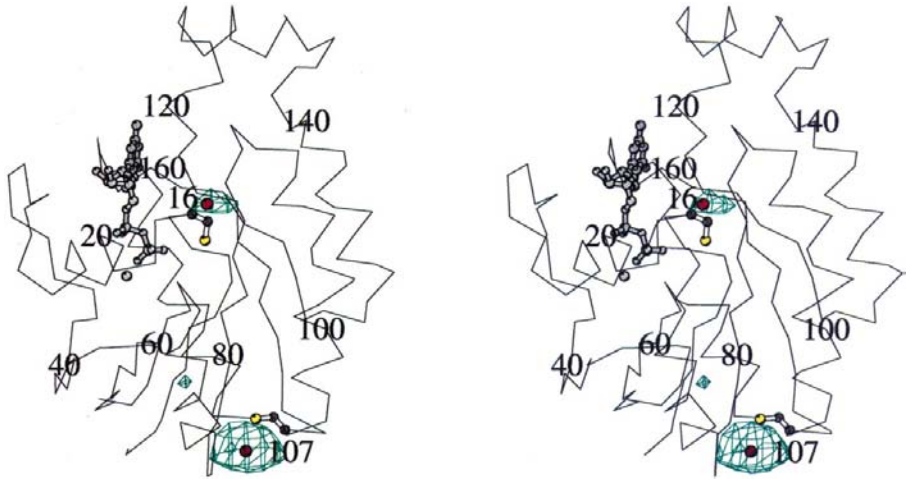

Figure 2
Difference Fourier map showing the peaks corresponding to the Hg sites. A stereoview of the map using the MAD phases is contoured in green at the 5σ level and is shown in relation to the position of RhoA. The C^{α} trace of RhoA is shown with Mg^{2+}–GDP and two mercury sites (red) are shown by the side chains of Cys16 and Cys107.

temperature-factor (B) correction to the native data was evaluated using *X-PLOR* and the optimal non-zero values for the tensor elements were $B_{11} = -86.4$, $B_{22} = -86.4$, $B_{33} = -1.1$ and $B_{12} = -65.2$.

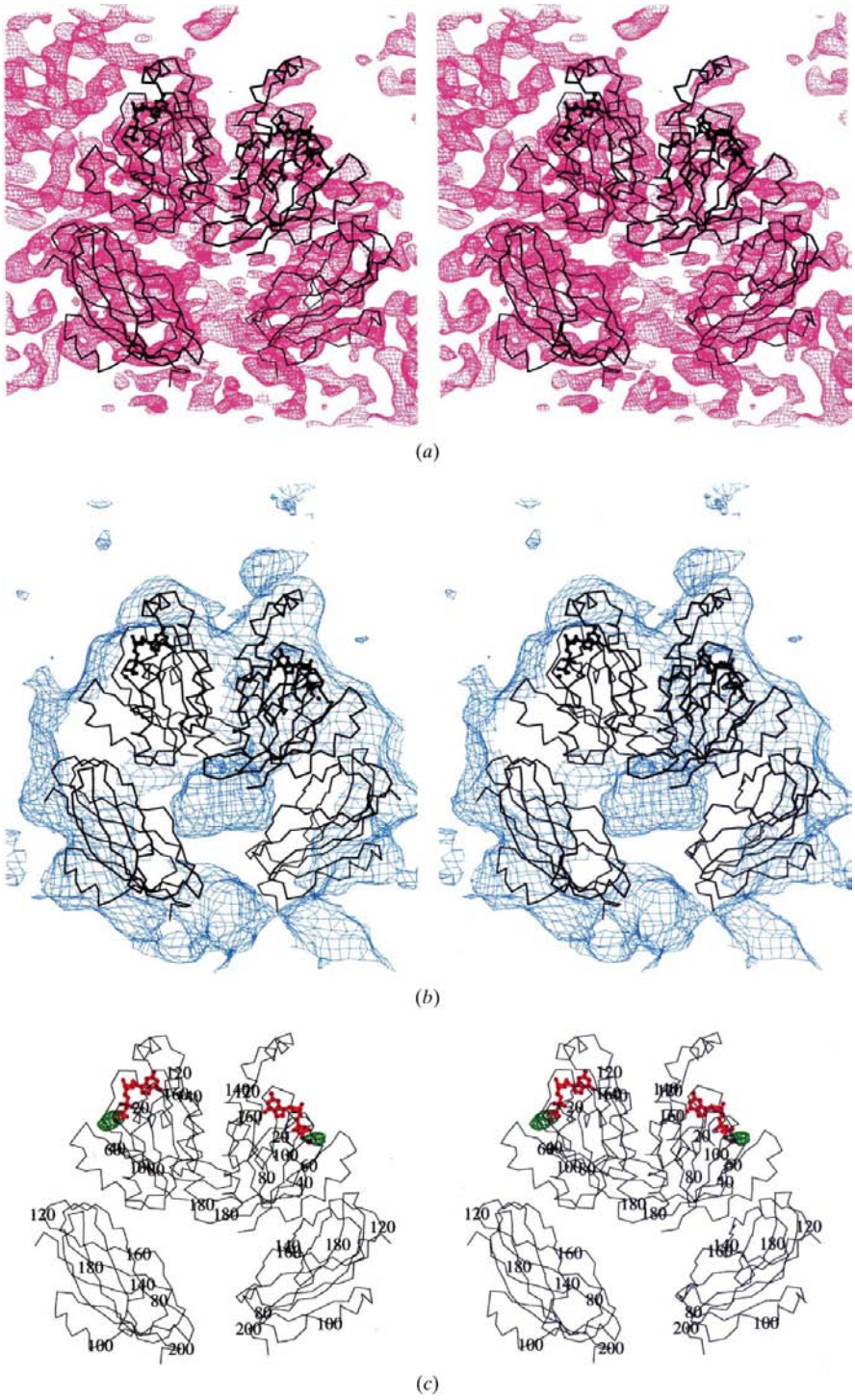

Figure 3
The experimentally phased 5 Å electron-density map of the RhoA–RhoGDI complex. (*a*) A slab of density contoured at a level of 1σ is shown in stereo. A C^{α} trace of the four protein molecules in the asymmetric unit is also shown. (*b*) A map of the correlation for the electron density related by the non-crystallographic symmetry is contoured at 2σ. (*c*) A Ho^{3+} difference electron-density map, contoured at 5σ and calculated with phases from the model and the isomorphous differences between native and Ho derivative data, is shown in green. This figure was prepared using *BOBSCRIPT* (Esnouf, 1997).

As already pointed out, none of the two individual models produced interpretable solutions. However, a dimer of RhoA constructed in accordance with the experimental electron-density map gave a clear solution, which was visibly enhanced when data were corrected for anisotropy. With the two RhoA molecules fixed and using the data corrected for anisotropy, the first RhoGDI molecule was successfully positioned, followed by the second one. In both cases, the correct solution had the highest correlation coefficient and lowest conventional R factor.

2.7. Miscellaneous calculations

The secondary structure of the N-terminal fragment of RhoGDI was predicted using *PredictProtein* (http://www.embl-heidelberg.de/services/sander/predictprotein/). Surface-area calculations and representations were calculated using the program *GRASP* (Nicholls *et al.*, 1991). Ribbon diagrams and figures containing electron density were produced with *BOBSCRIPT* (Esnouf, 1997).

3. Results and discussion

3.1. The yeast-expressed RhoA–RhoGDI complex as a model for the cytosolic species

The final protein preparation was very pure and appeared on a silver-stained gel as two bands of approximately equal density corresponding to RhoA and RhoGDI (Fig. 4*a*). We established that this tagged complex was indeed functionally representative of the wild-type cytosolic species. The association of RhoGDI with RhoA requires post-translational geranylgeranylation at the carboxyl terminus of RhoA and removal of the last three residues (Hori *et al.*, 1991). Translocation to and association with the cellular membrane is also dependent upon prenylation. Consequently, the facts that coexpressed human RhoA and RhoGDI formed a heterodimeric complex *in vivo* and that excess RhoA was associated with the membrane fraction provided good evidence that the human RhoA was prenylated in yeast. The biological functionality of the yeast-produced human RhoA was assessed by its Ca^{2+}-sensitizing effect on the force developed by

Table 3
Phasing statistics (5.0 Å).

NCS averaging correlation coefficient = 0.89.

MAD phasing	Ho^{3+}(edge)	Ho^{3+}(peak)	Ho^{3+}(remote)
R_C (acentric/centric)†	—	0.88/0.79	0.88/0.77
R_C (ano)‡	0.86	0.82	0.88
Phasing power (acentric/centric)§	—	1.0/0.75	1.04/0.78

MIRAS phasing	Hg	Ho^{3+}(edge)
Sites (major/minor)	4/2	2
R_C (acentric/centric)†	0.89/0.85	0.89/0.83
Phasing power (acentric/centric)§	1.01/0.67	0.99/0.64

Mean figure of merit¶.

Resolution (Å)	13.4	9.8	8.1	7.0	6.3	5.8	5.3	5.0	Total
MAD	0.54	0.59	0.63	0.60	0.50	0.42	0.35	0.32	0.47
MIRAS	0.41	0.41	0.43	0.43	0.47	0.42	0.40	0.36	0.41
Combined	0.65	0.69	0.71	0.69	0.63	0.55	0.51	0.46	0.59
Solvent flattening	0.73	0.81	0.86	0.85	0.79	0.71	0.69	0.70	0.76
Reflections phased	396	594	725	832	933	1010	1094	1165	6749

† $R_C = \sum \big||F_{PH}| \pm |F_P| - |F_H|_{calc}\big| / \sum \big||F_{PH}| \pm |F_P|\big|$, where F_{PH} and F_P are the scaled structure-factor amplitudes of the derivative and native, respectively, and F_H is the heavy-atom structure factor. ‡ R_C (ano) = $[\sum(|D_{PH}| - |D_{PH}|_{calc})^2 / \sum(D_{PH})^2]^{1/2}$, where D_{PH} is the anomalous difference for F_{PH}. § Phasing power = $\langle F_H \rangle / \langle$lack of closure$\rangle$. ¶ Figure of merit = $\langle \sum P(\alpha) \exp(i\alpha) / \sum P(\alpha) \rangle$, where $P(\alpha)$ is the phase probability at the angle α.

Table 4
Molecular replacement (15–4.5 Å).

Values in parentheses are the top values for a false solution.

	Native data		Data corrected for anisotropy	
Search model	CC†	R value‡	CC†	R value‡
Real-space refined model	34.5 (17.7)	57.0 (61.9)	38.4 (19.0)	52.6 (59.1)
Reconstruction from components				
(i) 2 RhoA	28.8 (29.4)	59.0 (60.7)	32.0 (25.3)	54.8 (56.8)
(ii) (2 RhoA) fixed + RhoGDI	—	—	33.9 (32.2)	53.9 (55.1)
(iii) (2 RhoA + RhoGDI) fixed + RhoGDI	—	—	39.3 (34.1)	51.9 (54.1)

† CC = correlation coefficient. ‡ R value = $\sum |F - F(\text{calc})| / \sum F$, where F is the structure-factor amplitude.

permeabilized smooth muscle resulting from inhibition of the smooth muscle myosin phosphatase (data not shown); unprenylated RhoA does not have a significant Ca^{2+}-sensitizing effect (Gong *et al.*, 1996).

All of the bound nucleotide was GDP, with a ratio of 1.25 mol GDP to 1 mol RhoA–RhoGDI. The apparent super-stoichiometric amount of GDP is likely to arise from an underestimation of the protein concentration by the Bio-Rad protein assay. Nonetheless, this result indicated the homogeneity of the preparation and showed that all of the RhoA bound GDP and retained it in the presence of a high concentration of Mg^{2+}. Over the course of 4 d in the presence of high concentration of Mg^{2+}, none of the bound GDP was released from the complex (data not shown). This result was crucial for the success of crystallization, which requires the sample to be stable over a period of at least several days. When we replaced GDP with GTP at low concentrations of Mg^{2+}, the hydrolysis rate of the bound GTP in the complex was significantly slower when compared with the intrinsic GTPase activity of RhoA (Fig. 4*b*), as expected from earlier reports (Chuang *et al.*, 1993; Hancock & Hall, 1993; Hart *et al.*, 1992). The $t_{1/2}$ of hydrolysis of the initial amount of bound GTP was 4.5 h at 295 K, whereas free RhoA hydrolyzes GTP with a $t_{1/2}$ of 18 min (Self & Hall, 1995). The complex with the affinity tags exchanged [*i.e.* $(His)_6$–RhoA/FLAG–RhoGDI] had similar characteristics, indicating that the affinity tags on the individual components of the Rho–RhoGDI complex do not affect the functionality of the heterodimer.

3.2. The quality of the model and its validation

The optimization of crystallization conditions allowed preparation of crystals as large as 350 × 450 × 450 µm (Fig. 4*c*). This, along with the fine-tuned freezing protocol, extended the resolution from the original 10 Å to 3.5 Å, albeit with strong anisotropy (Fig. 5). The Bragg reflections extend beyond 3.5 Å only along the c^* axis, but barely exceed the resolution of 5 Å in the plane perpendicular to the sixfold axis. The non-zero values for the tensor elements, which quantify the observed anisotropy, are probably among the highest reported (B_{11} = −86.4, B_{22} = −86.4, B_{33} = −1.1 and B_{12} = −65.2). Although all theoretical data to 3.5 Å were initially processed for the native crystal, higher resolution shells exhibited very poor statistics owing to lack of observed data along a^* and b^* at higher resolution, and consequently a cutoff limit of 4.0 Å was applied (Table 1). This extreme anisotropy constituted a serious difficulty, making it effectively impossible to refine an atomic model of the complex. However, given that the structures of both RhoA–GDP and of the C-terminal domain of RhoGDI are known from other investigations, we felt that it was justifiable to pursue the question of the mutual disposition of the two proteins in the complex, even with data to a limited resolution.

Out of necessity, the model which we propose is largely qualitative. Nonetheless, we are confident that within the limits imposed by the resolution it is accurate and yields important insight into the mechanism by which RhoGDI binds to RhoA. It is of particular importance that the mutual disposition of the two molecules in the complex has been cross-validated using various approaches. The original docking of the two molecules was carried out based on the experimentally phased (MAD plus MIR) electron density; the

helices of RhoA were readily recognizable in the electron density and were related by an obvious non-crystallographic dyad (Fig. 3). When the protein moiety of RhoA was thus placed, it was found that the positions of the two Ho^{3+} sites identified by Patterson methods coincided with the expected Mg^{2+}. Difference density for these Ho^{3+} sites is returned using model phases, lending further credibility to the model (Fig. 3*c*). There is also significant positive density which can easily be interpreted as the bound GDP nucleotide. Finally, the four major Hg^{2+} sites located by difference Fourier using the MAD phases were located in the immediate proximity of the free sulfhydryls of Cys16 and Cys107 in each of the two RhoA molecules (Fig. 2).

Although a single RhoA molecule does not yield a solution in *AMoRe*, a dimer of two RhoA molecules, as observed in the experimentally phased map, gives a clear solution. The two RhoGDI molecules can be positioned independently using *AMoRe*, and the result is very close to the manual docking into the experimental density. In fact, the root-mean-square difference calculated using all the atoms between the manually constructed complex refined by real-space methods against the experimentally phased map and the one generated by MR was only 1.15 Å for all atoms.

Meaningful refinement of atomic coordinates is not feasible at the resolution limit of 4.0–5.0 Å, but nevertheless attempts to refine the two components of the complex yielded improved agreement statistics. Torsion-angle dynamics with the maximum-likelihood target function in *CNS* improved the conventional *R* factor from 51 to 41% (free *R* factor from 51 to 47%) using data greater than 3σ between 8 and 4.0 Å. However, electron-density maps calculated with coefficients derived from the model refined at 4.0 Å showed little improvement over the experimentally phased map; these were suspected to have strong model bias and were not used.

We conclude that the mutual disposition of the two molecules in the complex has been accurately determined. However, the resulting coordinates of the complex obtained by docking of the existing models do not reflect any local changes which might have occurred in either RhoA or RhoGDI in response to the formation of the heterodimer.

Fortuitously, the experimental electron density also allowed the identification of those structural elements for which no high-resolution crystallographic models exist, *i.e.* the N-terminal fragment of RhoGDI and the C-terminal oligopeptide of RhoA. These are described in a qualitative way based on the residual experimental electron density, as described in §2.5, and C^{α} coordinates were generated for the N-terminus of RhoGDI and C-terminus of RhoA. No coordinates were generated for the geranylgeranyl moiety, which is presumed to occupy the internal cavity in RhoGDI.

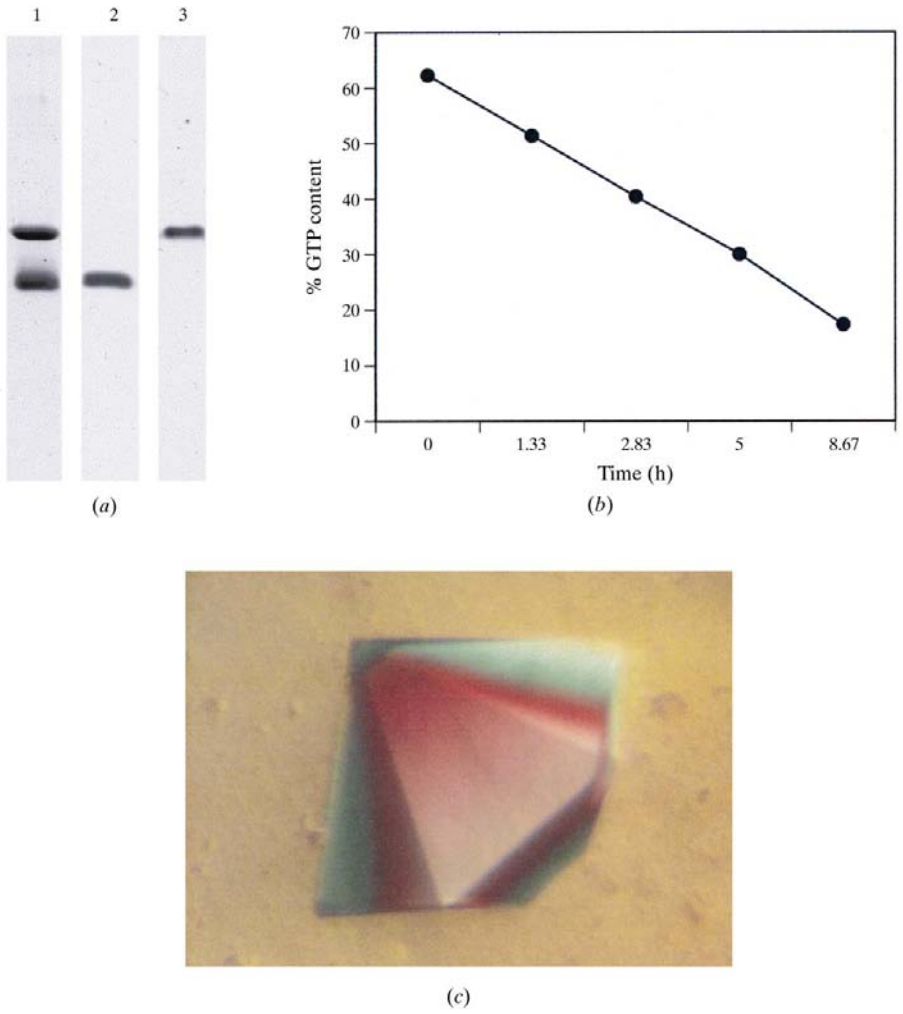

Figure 4
Characterization of the recombinant human RhoA–RhoGDI complex. (*a*) SDS–PAGE analysis of purified FLAG–RhoA/(His_6)–RhoGDI complex. Proteins were visualized by Coomassie staining of the 15% polyacrylamide gel (lane 1, 15 µg loaded) or by Western blotting with an anti-RhoA monoclonal antibody (lane 2, 50 ng loaded) or with an anti-RhoGDI polyclonal antibody (lane 3, 2.5 ng loaded) and visualized by chemiluminescence with the Amersham ECL kit. (*b*) Inhibition of intrinsic RhoA GTPase activity by Rho–GDI. GTP was exchanged into 0.1 m*M* purified FLAG–RhoA/(His_6)–RhoGDI complex with 2.5 m*M* GTP in 0.1 *M* Tris–HCl, 0.1 *M* NaCl, 5 m*M* $MgCl_2$ and 10 m*M* EDTA pH 7.6 at 295 K. After 3 h incubation, the $MgCl_2$ concentration was adjusted to 12.5 m*M* and the protein was passed through a desalting column to remove unbound nucleotide and exchanged into pH 8.0 buffer consisting of 0.1 *M* Tris–HCl, 0.1 *M* NaCl and 5 m*M* $MgCl_2$. The protein was concentrated to 50–100 m*M* and incubated at 295 K; aliquots were removed at the times indicated and the bound nucleotide was determined. The initial level of GTP bound to the complex was 60%. The $t_{1/2}$ of hydrolysis of bound GTP, determined from duplicate experiments, was 4.5 h. (*c*) A single crystal of the RhoA–GDP–RhoGDI complex.

3.3. Binding of the C-terminal domain of RhoGDI to RhoA

The crystallographic model of the RhoA–RhoGDI complex obtained by the docking of the models of RhoA–GDP (residues 4–180) and of the C-terminal domain of Rho–GDI (68–203) into an experimentally phased electron-density map provides the first insight into the nature of the interactions between the two proteins. The complex forms an elongated structure with a long axis of approximately 77 Å from the insert helix of RhoA, which is distal to the RhoGDI binding site, to the C-terminus of RhoGDI (Fig. 6). The GTPase-binding epitope of RhoGDI includes primarily residues in the *D–E* and *F–G* loops (nomenclature according to Gosser *et al.*, 1997) which join the respective β-strands in the immunoglobulin-like fold. Residues within 5 Å of RhoA include Glu121, Ile122, Ser124 and Gly125 in the *D–E* loop, as well as Met145, Gly147, Ser148 and Gly150 in the *F–G* loop. In addition, Asp184, which is in the *H–I* loop, is also within 5 Å of RhoA. This epitope, conserved in the RhoGDI family, is consistent with earlier NMR experiments using non-prenylated Cdc42Hs–GDP and ^{15}N RhoGDI (Gosser *et al.*, 1997).

Our study reveals for the first time the epitope on RhoA which binds to the C-terminal domain of RhoGDI; it includes

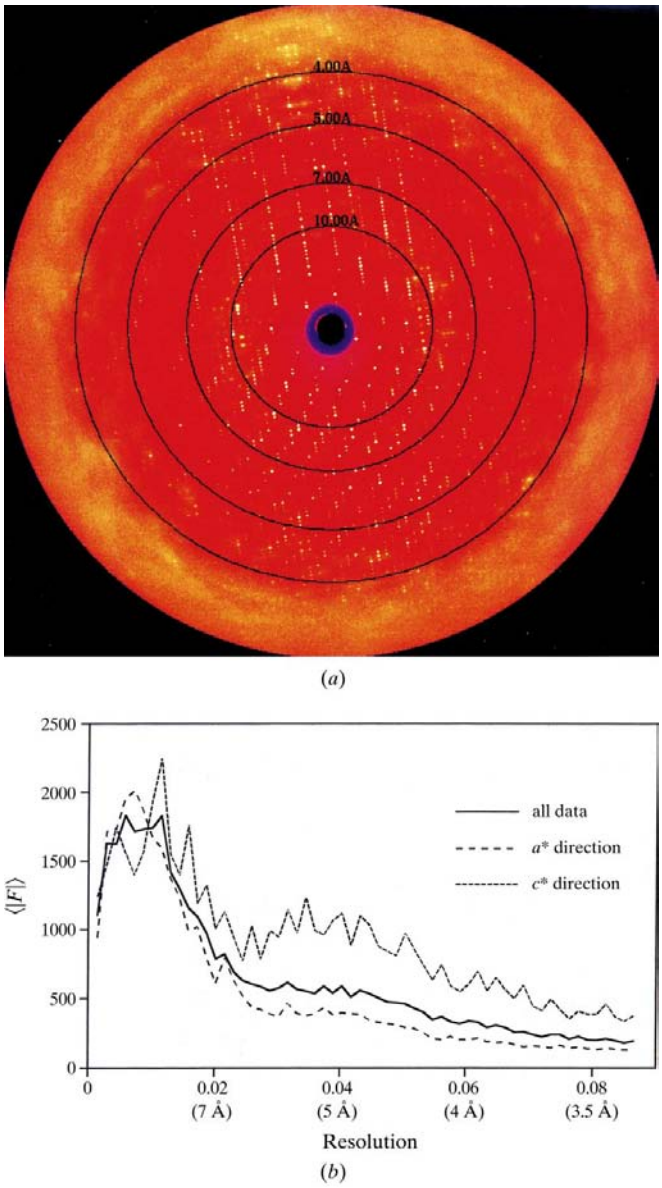

Figure 5
(*a*) A representative data frame (1° oscillation range) from the native data set collected at the EMBL Outstation, Hamburg (see Table 1 for details). The sixfold axis is approximately vertical. Note the extreme anisotropy in the image. (*b*) Mean structure-factor amplitude as a function of resolution and direction in the native data set. The data are plotted in units of $4[(\sin\theta)/\lambda]^2$, and the corresponding crystal lattice spacing is labeled. A plot of all data (20 454 reflections) is shown as a solid line, and the two broken lines are plots for two sets of reflections selected within a 30° cone oriented along the reciprocal-lattice axes *a** or *c**, with 7743 and 3029 reflections, respectively.

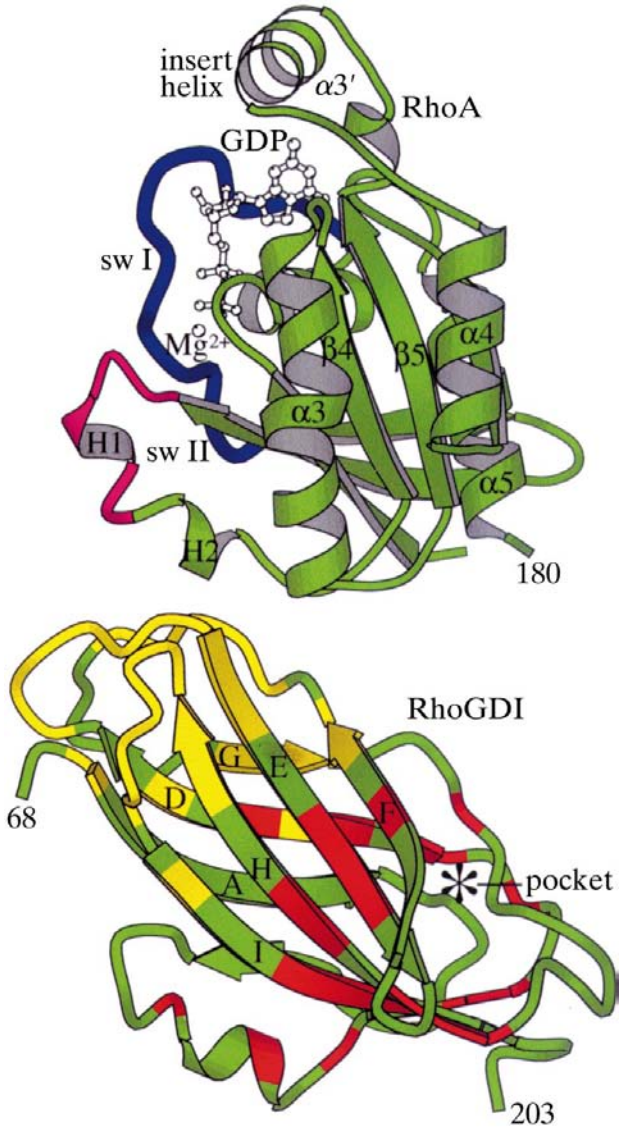

Figure 6
Ribbon diagram of the RhoA–RhoGDI complex. A schematic view of the mutual disposition of the RhoA GTPase and the C-terminal domain of RhoGDI is shown. Highlighted in the RhoGDI molecule are the locations of residues identified by NMR experiments (Gosser *et al.*, 1997) which were shown to be affected by addition of a prenylated peptide (red) or non-isoprenylated Cdc42Hs (yellow). This figure was prepared using *BOBSCRIPT* (Esnouf, 1997).

residues at the base of the switch II region and in the neighboring helix α3. The amino acids of RhoA which are within 5 Å of RhoGDI in the model are the switch II residues Arg68, Leu69, Pro71, Leu72 and Pro75, and residues His105, Phe106 and Pro108 from helix α3. With the exception of Phe106, replaced by His in Rac and Cdc42Hs, all these residues are conserved throughout the Rho family, but are not found in the Ras GTPases. Lack of highly refined coordinates precludes a detailed characterization of the contacts between specific amino acids, but the model does allow for the identification of some potentially important interactions. A hydrophobic cluster is formed between Ile122 of RhoGDI and the RhoA residues Leu69 and Leu72. A hydrophobic interaction may also exist between Met145 of RhoGDI and Pro108 of RhoA. The side chain of Phe106 from RhoA packs against Gly125 and Gly147 in RhoGDI, which form a groove on the surface of the molecule. Finally, Asp184 of RhoGDI and His105 of RhoA are close enough in the model to suggest a possible hydrogen bond.

Given the high affinity of Rho and RhoGDI proteins for one another [the representative Cdc42Hs–GDI interaction has an apparent K_d value of 30 nM (Nomanbhoy & Cerione, 1996)] the area of contact between the molecules in the complex is relatively small, being 413 Å^2 in each of the proteins. This implies that the contribution of this contact to the overall binding energy is relatively small. The critical contribution is more likely to originate from the binding of the geranylgeranyl moiety within the hydrophobic cavity of the C-terminal domain of RhoGDI. Indeed, non-prenylated RhoA is not bound by RhoGDI (Hori *et al.*, 1991), while a replacement of Ile by Asp at position 177 in RhoGDI, an amino acid located at the entrance of the lipid-binding cavity and away from the GTPase, reduces the affinity of Cdc42Hs for RhoGDI by a factor of 20 (Platko *et al.*, 1995). In the crystal structure of the complex, the distance from the C-terminus of RhoA to the entrance of the hydrophobic pocket of RhoGDI is approximately 25 Å. The entrance to the pocket faces the C-terminal helix in RhoA in such a way that no conformational changes are required to dock the lipid to RhoGDI. Ten residues are missing from the C-terminus of the RhoA model, and in the complex they probably continue as a helix for one more turn and then assume an extended conformation. This is corroborated by the residual electron-density map, which shows an extension of positive density from the C-terminal helix of RhoA directly towards the opening to the pocket in RhoGDI. A difference electron-density map calculated with the coefficients $F_{obs} - F_{calc}$ and experimental phases (data not shown) reveals significant positive density inside the pocket, consistent with a bound geranylgeranyl group.

3.4. Binding of the N-terminal oligopeptide of RhoGDI to the GTPase

Perhaps the most important question with respect to the structure of RhoGDI is the conformation of its N-terminal oligopeptide, residues 1–63, in the complex with RhoA. Residues 1–22 are not required for the biological functions of RhoGDI and are probably disordered (Platko *et al.*, 1995), while residues 23–59, which are required for the inhibition of nucleotide dissociation/exchange and extraction of the GTPase from membrane, are also disordered in the native molecule but not in the complex (Gosser *et al.*, 1997; Keep *et al.*, 1997).

The experimental electron-density map of the complex contains additional positive density to that corresponding to the RhoA and the C-terminal domain of RhoGDI. To better visualize these features, we subtracted the density associated with the protein moieties from the density of the intact complex. We refer to the density map obtained in this way as residual density. Fig. 7 shows the result of this calculation. A long stretch of continuous density wraps around the RhoA molecule and connects with the N-terminus of the RhoGDI molecule. This density begins adjacent to RhoA at the end of helix α3 by residues Glu102 and Lys104 and extends across to the helical switch II region over Pro71. The density then makes a sharp turn, assumes a cylindrical shape and runs adjacent to the switch II helix over Arg68 and Tyr66. A sharp turn follows, and a second cylindrical fragment runs in close proximity to Thr37 in the switch I region, over Val38 and Glu40 and adjacent to the side chain of Asn41 before turning toward the C-terminal domain of RhoGDI.

Fig. 8 shows a model for residues 24–68 in RhoGDI based on the residual density. It contains a stretch of extended chain, two short α-helices connected by a short linker and a loop which connects this fragment with the N-

Figure 7
Residual density corresponding to the N-terminus of RhoGDI. A stereoview of the residual electron density is contoured at a level corresponding to 1σ of the original map shown in Fig. 3. The model is rotated about the vertical axis relative to Fig. 6.

terminus of the immunoglobulin-like domain. It is interesting that in the crystal structure of the C-terminal domain of RhoGDI (Keep *et al.*, 1997), the second copy of the three molecules in the asymmetric unit adopts the conformation for residues 60–68 which follows the electron density observed here in the complex. Secondary-structure prediction supports the model, as the two fragments in the N-terminal oligopeptide between residues 32–41 and 46–55 have strong helical propensities. These fragments agree with respect to the lengths and positions along the polypeptide chains of the helices inferred from the electron-density map (Fig. 9). The putative four-residue linker would also appear to be of appropriate length to connect the helices. Thus, in summary, the model suggests that upon binding to the Rho GTPase, residues 23–59 become ordered and fold into an extended structure followed by two α-helices. None of these fragments makes any contact with each other or with the C-terminal domain of RhoGDI. Therefore, in the absence of the GTPase, their mutual disposition is no longer stable. Whether the helices remain intact in free RhoGDI is not clear, since HSQC spectra reported in the literature (Gosser *et al.*, 1997; Keep *et al.*, 1997) are unlikely to differentiate between a free-floating helix and a completely extended structure.

3.5. Dimerization of complexes

The asymmetric unit contains two complexes related by the NCS twofold axis. This crystal packing brings the two RhoA molecules into close proximity, whereas the RhoGDI molecules make contact exclusively with molecules related by crystallographic symmetry. The RhoA molecules interact across the surface formed by α4- and α5-helices, with the β6-strand sandwiched between them. The intermolecular packing appears to be dominated by electrostatic interactions between the α4-helix of one RhoA molecule and the α5-helix of the other. Although the detailed interactions cannot be elucidated with the present data, the residues from helix α4 which are likely to participate in this interaction are Glu142, Arg145, Asp146 and Asn149. Similarly, those residues from helix α5 which are likely to be important for the NCS interaction include Glu169, Glu172, Met173 and Arg176. Side chains of residues from the β6-strand which would contribute to the interacting surface are Phe154, Tyr156, Met157 and Glu158. Although this packing results in a dimerization of complexes, such dimerization is not known to be biologically relevant.

3.6. Cytophysiological implications

RhoGDI has been reported to have three functions. It inhibits the nucleotide exchange catalyzed by guanine nucleotide-exchange factors (GEFs), decreases the intrinsic rate of GTP hydrolysis by the GTPase and extracts the Rho GTPase from the membrane. Earlier structural studies of RhoGDI (Gosser *et al.*, 1997; Keep *et al.*, 1997) revealed the tertiary structure of its C-terminal domain and suggested the mechanism by which the geranylgeranyl group of the GTPase is bound, but could not rationalize its other functional properties. The present crystallographic analysis sheds considerable light on the structure–function relationships which govern the Rho–RhoGDI interactions.

Upon formation of the complex with the GTPase, the N-terminal fragment of RhoGDI (23–59) wraps around a surface epitope on RhoA which includes fragments of the switch I and switch II regions. In particular, it comes into close contact with Thr37, a residue which plays a key role in the nucleotide-exchange mechanism catalyzed by Rho-specific, Dbl-like GEFs (Li & Zheng, 1997). The RhoA–GDP crystal structure (Wei *et al.*, 1997) showed that, in contrast to Ras, Thr37 in RhoA is directly involved in the coordination of Mg^{2+} through the main-chain carbonyl group. When Thr37 of RhoA or the corresponding Thr35 in Cdc42Hs is mutated to an Ala, there is complete loss of sensitivity to GEFs in the GTPases (Li & Zheng, 1997). In Ras, an analogous mutation of Thr35 to Ala produces only about a threefold reduction in sensitivity to Cdc25, a Ras-specific GEF (Mistou *et al.*, 1992). It can therefore be assumed that Dbl-like GEFs operate by a mechanism which involves the disruption of the interaction between the carbonyl of Thr37 and Mg^{2+}, leading to the dissociation of Mg^{2+} and concomitant loss of GDP. RhoGDI inhibits this function by shielding the side chain of Thr37 in its complex with Rho GTPases.

In order for RhoGDI to act on diverse Rho-family members, the epitope responsible for the binding of the inhibitory N-terminal fragment of RhoGDI ought to be conserved among the GTPases. Fig. 10 shows the sequence conservation for RhoA, RhoB, RhoC, Rac1, Rac2 and

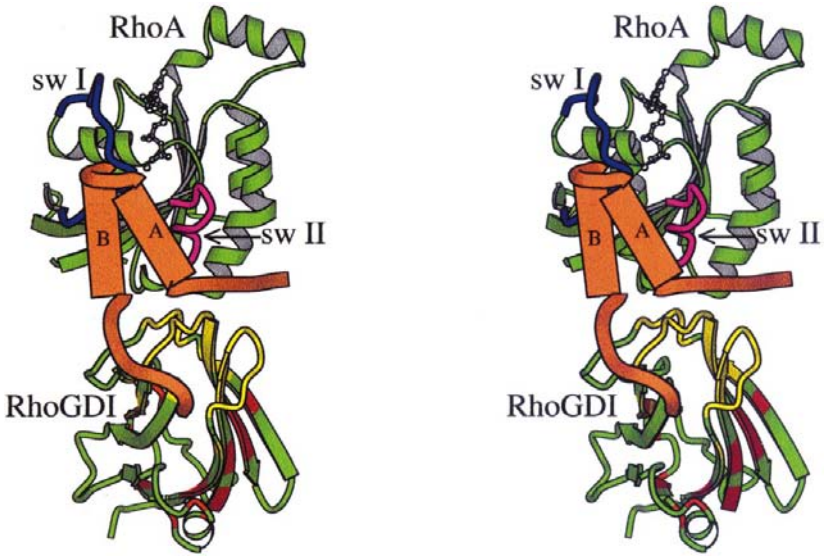

Figure 8
Model of the complex with the N-terminal fragment of RhoGDI. A model which follows the residual density is highlighted in orange and is shown from the same view as in Fig. 7.

Cdc42Hs. It is evident that the surface of RhoA covered by the N-terminal fragment of RhoGDI consists almost exclusively of very highly conserved amino acids. A similar analysis of the sequences for the RhoGDI family is not possible because of the uncertainty in the exact orientation of specific residues in RhoGDI with respect to the GTPase. We note, however, that the hydrophobic faces of the helices, which are most likely to interact with the GTPases, are largely conserved (Fig. 9) and the small variations in sequences could potentially account for the differences in affinity between the various isoforms of RhoGDI for Rho GTPases.

The inhibition of the intrinsic RhoA GTPase activity by RhoGDI is more difficult to explain, and a structure of the complex involving a GTP analogue bound to Rho will be required to address this question in detail. However, the present study suggests that the N-terminal fragment of RhoGDI is likely to stabilize the conformations of the switch I and switch II residues and thereby confer additional stability on the Rho–GTP complex.

It is also necessary to address the mechanism by which RhoGDI solubilizes Rho. The truncated, Δ59 mutant of RhoGDI fails to extract Cdc42Hs from the membranes (Gosser *et al.*, 1997), indicating that the binding of the geranylgeranyl group by RhoGDI is not sufficient for its extraction from the membrane. The N-terminal fragment may interact with the GTPase first and may reorient the protein in such a way that the geranylgeranyl group becomes accessible to RhoGDI. Such a mechanism agrees with the recently proposed two-step kinetics by which RhoGDI extracts Cdc42Hs from the membrane (Nomanbhoy *et al.*, 1999).

There are some inconsistencies between the molecular model of the Rho–RhoGDI complex inferred from our investigation and earlier studies which probed the nature of the interactions between the two proteins. The native RhoA–RhoGDI complex obtained from rabbit ileum cytosol cannot be immunoprecipitated using antibodies raised against the insert helix of RhoA (Fujihara *et al.*, 1997). However, following additional chromatographic purification, native partially purified RhoA–RhoGDI complex, as well as the recombinant yeast-produced complex, could be immunoprecipitated with the same antibody (data not shown). The combination of this finding with the proposed structure of the complex, which shows that the insert helix is distal to the RhoGDI binding site, suggests that the lack of immunoprecipitability of the crude native complex does not result from the shielding of the antibody-binding epitope by RhoGDI, but more likely from the presence of other as yet unidentified protein(s) in the complex. Finally, the replacement of the insert helix in Cdc42Hs with the short link adapted from Ras implicated this helix in the inhibitory function of RhoGDI (Wu *et al.*, 1997). This suggestion cannot be rationalized by the crystal structure and suggests secondary effects arising from the conformational changes in the modified Cdc42Hs protein.

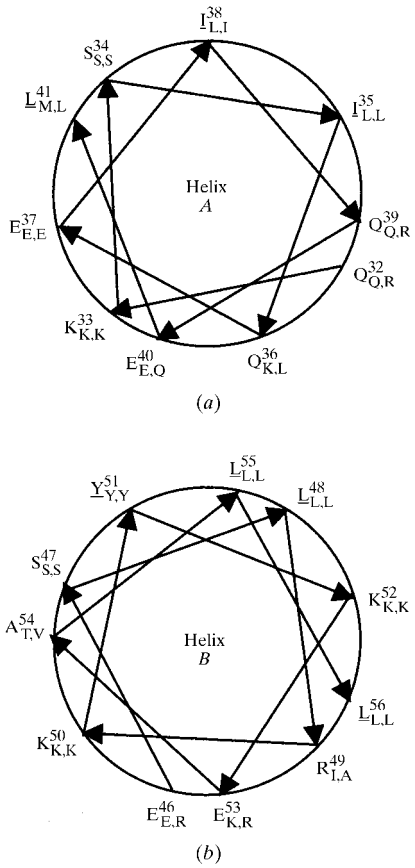

Figure 9
Helical wheel projections are shown for two predicted helices between residues 32 and 56. Amino acids for RhoGDI are labeled on the outside of the wheel, along with subscripts which identify the corresponding amino-acid residues in the sequences for RhoGDIβ and RhoGDIγ.

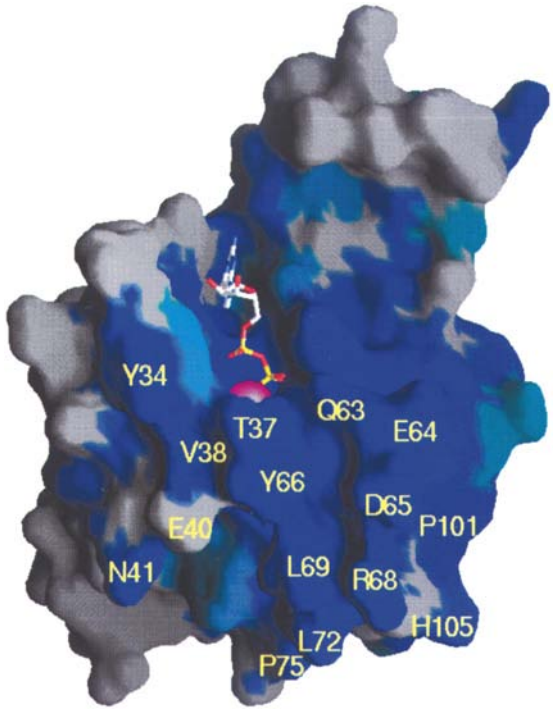

Figure 10
Amino-acid sequence conservation is represented on the surface of RhoA as a gradation from gray to dark blue, corresponding to 100% conservation [figure prepared using *GRASP* with modifications as described by Soisson *et al.* (1998)].

In conclusion, the proposed model of the recombinant RhoA–RhoGDI complex sheds new light on the mechanism by which RhoGDI carries out its biological functions and particularly the mechanism by which RhoGDI inhibits nucleotide exchange. Nonetheless, further work will be required to address the details of the interactions, elusive at the low resolution imposed by the crystals, and to reconcile the structure of the purified complex with its behavior in cytosolic extracts. This work is in progress in our laboratories.

The project was funded by the NIH Program Project Grant HL48807. We would like to thank Dr A. Kiyatkin for advice regarding protein crystallization, Dr M. Gong for the help with Fig. 1, Dr John Bushweller for discussions, Drs W. Minor and Z. Otwinowski for help with data collection at APS, and EMBL Outstation Hamburg for synchrotron time allocation. Drs A. Hall and G. Bokoch kindly provided the genes used in this work. Use of the Argonne National Laboratory Structural Biology Center beamline at the Advanced Photon Source was supported by the US Department of Energy, Office of Energy Research, under contract No. W-31-109-ENG-38.

References

Adra, C. N., Iyengar, A. R., Syed, F. A., Kanaan, I. N., Rilo, H. L., Yu, W., Kheraj, R., Lin, S. R., Horiuchi, T., Khan, S., Weremowicz, S., Lim, B., Morton, C. C. & Higgs, D. R. (1998). *Genomics*, **53**, 104–109.

Barrett, T., Xiao, B., Dodson, E. J., Dodson, G., Ludbrook, S. B., Nurmahomed, K., Gamblin, S. J., Musacchio, A., Smerdon, S. J. & Eccleston, J. F. (1997). *Nature (London)*, **385**, 458–461.

Bokoch, G. M., Bohl, B. P. & Chuang, T. H. (1994). *J. Biol. Chem.* **269**, 31674–31679.

Bourmeyster, N., Stasia, M. J., Garin, J., Gagnon, J., Boquet, P. & Vignais, P. V. (1992). *Biochemistry*, **31**, 12863–12869.

Brunger, A. T., Adams, P. D., Clore, G. M., DeLano, W. L., Gros, P., Grosse-Kunstleve, R. W., Jiang, J. S., Kuszewski, J., Nilges, M., Pannu, N. S., Read, R. J., Rice, L. M., Simonson, T. & Warren, G. L. (1998). *Acta Cryst.* D**54**, 905–921.

Chuang, T. H., Xu, X., Knaus, U. G., Hart, M. J. & Bokoch, G. M. (1993). *J. Biol. Chem.* **268**, 775–778.

Collaborative Computational Project, Number 4 (1994). *Acta Cryst.* D**50**, 760–763.

Esnouf, R. M. (1997). *J. Mol. Graph.* **15**, 132–143.

Feltham, J. L., Dotsch, V., Raza, S., Manor, D., Cerione, R. A., Sutcliffe, M. J., Wagner, G. & Oswald, R. E. (1997). *Biochemistry*, **36**, 8755–8766.

Fujihara, H., Walker, L. A., Gong, M. C., Lemichez, E., Boquet, P., Somlyo, A. V. & Somlyo, A. P. (1997). *Mol. Biol. Cell*, **8**, 2437–2447.

Fukumoto, Y., Kaibuchi, K., Hori, Y., Fujioka, H., Araki, S., Ueda, E., Kikuchi, A. & Takai, Y. (1990). *Oncogene*, **5**, 1321–1328.

Gamblin, S. J. & Smerdon, S. J. (1998). *Curr. Opin. Struct. Biol.* **8**, 195–201.

Gong, M. C., Fujihara, H., Somlyo, A. V. & Somlyo, A. P. (1997). *J. Biol. Chem.* **272**, 10704–10709.

Gong, M. C., Fujihara, H., Walker, L. A., Somlyo, A. V. & Somlyo, A. P. (1997). *Mol. Biol. Cell*, **8**, 279–286.

Gong, M. C., Iizuka, K., Nixon, G., Browne, J. P., Hall, A., Eccleston, J. F., Sugai, M., Kobayashi, S., Somlyo, A. V. & Somlyo, A. P. (1996). *Proc. Natl Acad. Sci. USA*, **93**, 1340–1345.

Gosser, Y. Q., Nomanbhoy, T. K., Aghazadeh, B., Manor, D., Combs, C., Cerione, R. A. & Rosen, M. K. (1997). *Nature (London)*, **387**, 814–819.

Hancock, J. F. & Hall, A. (1993). *EMBO J.* **12**, 1915–1921.

Hart, M. J., Maru, Y., Leonard, D., Witte, O. N., Evans, T. & Cerione, R. A. (1992). *Science*, **258**, 812–815.

Hirshberg, M., Stockley, R., Dodson, G. & Webb, R. (1997). *Nature Struct. Biol.* **4**, 147–151.

Hori, Y., Kikuchi, A., Isomura, M., Katayama, M., Miura, Y., Fujioka, H., Kaibuchi, K. & Takai, Y. (1991). *Oncogene*, **6**, 515–522.

Ihara, K., Muraguchi, S., Kato, M., Shimizu, T., Shirakawa, M., Kuroda, S., Kaibuchi, K. & Hakoshima, T. (1998). *J. Biol. Chem.* **273**, 9656–9666.

Itoh, K., Yoshioka, K., Akedo, H., Uehata, M., Ishizaki, T. & Narumiya, S. (1999). *Nature Med.* **5**, 221–225.

Jalink, K., van Corven, E. J., Hengeveld, T., Morii, N., Narumiya, S. & Moolenaar, W. H. (1994). *J. Cell. Biol.* **126**, 801–810.

Jones, T. A., Zou, J. Y., Cowan, S. W. & Kjeldgaard, M. (1991). *Acta Cryst.* A**47**, 110–119.

Keep, N. H., Barnes, M., Barsukov, I., Badii, R., Lian, L. Y., Segal, A. W., Moody, P. C. E. & Roberts, G. C. K. (1997). *Structure*, **5**, 623–633.

Kleywegt, G. J. & Jones, T. A. (1994). *Proceedings of the CCP4 Study Weekend. From First Map to Final Model*, edited by S. Bailey, R. Hubbard & D. A. Waller, pp. 59–66. Warrington: Daresbury Laboratory.

Li, R. & Zheng, Y. (1997). *J. Biol. Chem.* **272**, 4671–4679.

Luo, L., Jan, L. Y. & Jan, Y. N. (1997). *Curr. Opin. Neurobiol.* **7**, 81–86.

Mackay, D. J. G. & Hall, A. (1998). *J. Biol. Chem.* **273**, 20685–20688.

Mariot, P., O'Sullivan, A. J., Brown, A. M. & Tatham, P. E. (1996). *EMBO J.* **15**, 6476–6482.

Mistou, M. Y., Jacquet, E., Poullet, P., Rensland, H., Gideon, P., Schlichting, I., Wittinghofer, A. & Parmeggiani, A. (1992). *EMBO J.* **11**, 2391–2397.

Nakamoto, R. K., Rao, R. & Slayman, C. W. (1991). *J. Biol. Chem.* **266**, 7940–7949.

Narumiya, S. (1996). *J. Biochem.* **120**, 215–228.

Narumiya, S., Ishizaki, T. & Watanabe, N. (1997). *FEBS Lett.* **410**, 68–72.

Nassar, N., Hoffman, G. R., Manor, D., Clardy, J. C. & Cerione, R. A. (1998). *Nature Struct. Biol.* **5**, 1047–52.

Navaza, J. (1994). *Acta Cryst.* A**50**, 157–163.

Nicholls, A., Sharp, K. & Honig, B. (1991). *Proteins Struct. Funct. Genet.* **11**, 281–296.

Nomanbhoy, T. K. & Cerione, R. (1996). *J. Biol. Chem.* **271**, 10004–10009.

Nomanbhoy, T. K., Erickson, J. W. & Cerione, R. A. (1999). *Biochemistry*, **38**, 1744–1750.

Norman, J. C., Price, L. S., Ridley, A. J. & Koffer, A. (1996). *Mol. Biol. Cell*, **7**, 1429–1442.

Otwinowski, Z. & Minor, W. (1997). *Methods Enzymol.* **276**, 307–326.

Pan, J. Y. & Wessling-Resnick, M. (1998). *Bioessays*, **20**, 516–521.

Platko, J. V., Leonard, D. A., Adra, C. N., Shaw, R. J., Cerione, R. A., & Lim, B. (1995). *Proc. Natl Acad. Sci. USA*, **92**, 2974–2978.

Rittinger, K., Walker, P. A., Eccleston, J. F., Nurmahomed, K., Owen, D., Laue, E., Gamblin, S. J. & Smerdon, S. J. (1997). *Nature (London)*, **388**, 693–697.

Rittinger, K., Walker, P. A., Eccleston, J. F., Smerdon, S. J. & Gamblin, S. J. (1997). *Nature (London)*, **389**, 758–762.

Sasaki, T. & Takai, Y. (1998). *Biochem. Biophys. Res. Commun.* **245**, 641–645.

Scheffzek, K., Ahmadian, M. R., Wiesmuller, L., Kabsch, W., Stege, P., Schmitz, F. & Wittinghofer, A. (1998). *EMBO J.* **17**, 4313–4327.

Scheffzek, K., Ahmadian, M. R. & Wittinghofer, A. (1998). *Trends Biochem. Sci.* **23**, 257–262.

Self, A. J. & Hall, A. (1995). *Methods Enzymol.* **256**, 67–76.

Sheffield, P., Garrard, S. & Derewenda, Z. (1999). *Protein Expr. Purif.* **15**, 34–39.
Sheldrick, G. M. & Gould, R. O. (1995). *Acta Cryst.* B**51**, 423–431.
Soisson, S. M., Nimnual, A. S., Uy, M., Bar-Sagi, D. & Kuriyan, J. (1998). *Cell*, **95**, 259–268.
Sprang, S. R. (1997). *Curr. Opin. Struct. Biol.* **7**, 849–856.
Uehata, M., Ishizaki, T., Satoh, H., Ono, T., Kawahara, T., Morishita, T., Tamakawa, H., Yamagami, K., Inui, J., Maekawa, M. & Narumiya, S. (1997). *Nature (London)*, **389**, 990–994.
Wei, Y., Zhang, Y., Derewenda, U., Liu, X., Minor, W., Nakomoto, R. K., Somlyo, A. V., Somlyo, A. P. & Derewenda, Z. S. (1997). *Nature Struct. Biol.* **4**, 699–702.
Wissmann, A., Ingles, J., McGhee, J. D. & Mains, P. E. (1997). *Genes Devel.* **11**, 409–422.
Wu, W. J., Leonard, D. A., Cerione, R. A. & Manor, D. (1997). *J. Biol. Chem.* **272**, 26153–26158.
Yoshioka, K., Matsumura, F., Akedo, H. & Itoh, K. (1998). *J. Biol. Chem.* **273**, 5146–5154.